

# Spot activity and the differential rotation on HD 106225 derived from Doppler tomography

A.P. Hatzes

McDonald Observatory, The University of Texas at Austin, Austin, Texas 78712-1083, USA

Received 1 July 1997 / Accepted 24 September 1997

**Abstract.** Doppler images of the cool spot distribution on the RS CVn-type star HD 106225 are presented. These images, for Epoch 1995.14, were derived using four photospheric lines. The spot distribution is characterized by a large (radius =  $20^\circ$ ) spot at latitude  $45^\circ$  and a weak polar spot with an appendage. The polar spot is considerably smaller than similar features found on other RS CVn stars. The rotation rate as a function of latitude was derived by comparing the Doppler images of this work to one found for Epoch 1991.3 by Strassmeier. This rotation law is consistent to the one found by Strassmeier in that the differential rotation on HD 106225 is in the opposite sense as on the Sun and at least a factor of 10 less extreme. A comparison of the differential rotation rates derived from Doppler imaging of other spotted stars yields a linear relationship with the logarithm of the stellar rotation period; the longer the rotation period the faster the polar regions are rotating with respect to the equatorial regions. The crossover point between polar acceleration and equatorial acceleration occurs at a rotation period of about 2 days.

The full  $H\alpha$  emission (after subtracting the absorption component of an inactive star) shows sinusoidal variations with an amplitude of about  $10 \text{ km s}^{-1}$ , significantly less than the rotation rate of  $25 \text{ km s}^{-1}$ . This modulation is interpreted as arising from a plage located at high stellar latitude and adjacent to the polar appendage seen in the photospheric spot distribution.

**Key words:** stars: HD 106225; activity; rotation – starspots

## 1. Introduction

HD 106225 (= HU Virgo) is a late-type (K0 IV) single-lined spectroscopic binary that shows all the signs of RS CVn-type activity such as photometric variability due to cool star spots (Fekel et al. 1991) Ca II H and K emission (Bidelman 1981), and coronal X-rays, to name a few. Strassmeier (1994; hereafter S94) used the Doppler imaging technique to derive the cool spot distribution on this star for two epochs in 1991. These images revealed a cool polar spot with two large appendages. From an

analysis of the Ca II variations he also found evidence for two chromospheric plages separated  $180^\circ$  apart that seemed to be spatially related to the polar appendages. Broadening in the  $H\alpha$  profile suggested mass flow in a coronal loop connecting the two plage regions. Strassmeier also used UVB photometry to trace the spot evolution on HD 106225 in 1991 and he found evidence for a fairly stable spot distribution. The inferred differential rotation was a factor of 10 times less than that of the Sun and in the opposite sense - the poles of HD 106225 rotate faster than the equator. This low value of differential rotation is consistent with values derived from Doppler imaging of other RS CVn stars. UX Arietis showed surface differential rotation a factor of 10 less than the Sun (Vogt & Hatzes 1991), and HR 1099 showed differential rotation a factor of 50 less than in the Sun (Vogt & Hatzes 1996; Vogt et al. 1997). Whereas EI Eridani showed evidence for equatorial acceleration (Hatzes & Vogt 1992), the other RS CVn-type stars had polar regions rotating faster than the equator.

An important aspect of any Doppler imaging study of an active late-type star is obtaining a series of images for a given star covering a wide time base. These are important for establishing migration patterns, measuring differential rotation rates, and discerning activity cycles. In this paper a Doppler image of HD 106225 is presented for Epoch 1995.14 and this is compared to the earlier image derived by S94.

## 2. Data acquisition

Data were acquired using the 2.1-m telescope at McDonald Observatory and the Sandiford Echelle Spectrometer. This prism cross-dispersed echelle spectrometer provides large wavelength coverage (up to  $1500 \text{ \AA}$ ) at a resolving power of 60,000 (two pixel slit) when used with a Reticon Corporation  $1200 \times 400$  CCD detector (McCarthy et al. 1993). For the observations of HD 106225 the instrument was set up to cover the spectral region of  $5800 - 7200 \text{ \AA}$ . Table 1 lists the journal of observations which include Julian Day of mid-exposure, exposure time, signal-to-noise per pixel and rotation phase. Phases were reckoned using the orbital ephemeris of S94:

$$JD = 2,448,375.25 + 10.38758E. \quad (1)$$

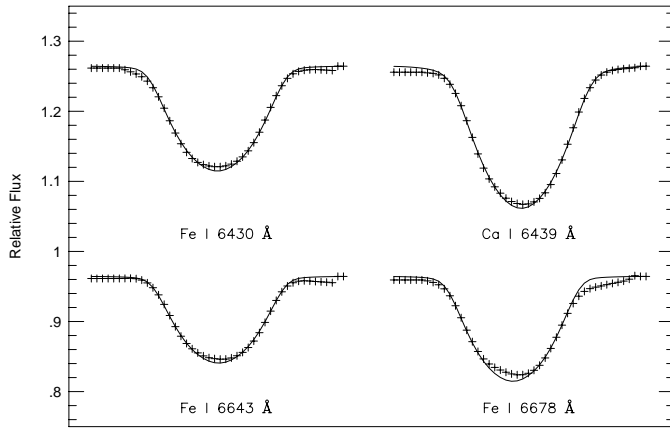


**Fig. 1.** (crosses) The mean spectral line profiles for the four photospheric lines used for Doppler imaging. The crosses are the observed data and the line is a synthetic rotationally broadened line profile.

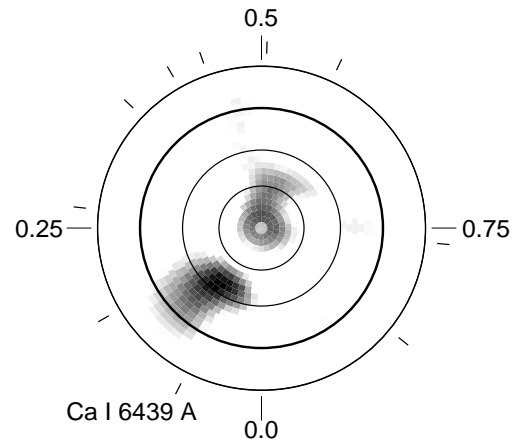


**Fig. 3.** Doppler image derived using Ca I 6439 Å. The darkest regions correspond to a temperature 820 K below the photospheric value.

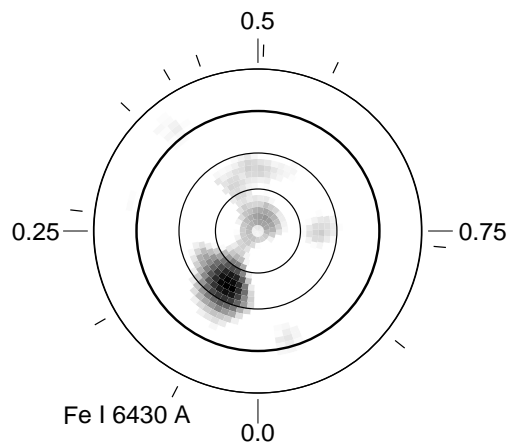


**Fig. 2.** The Doppler image derived using the Fe I 6430 Å line. The image is shown in a flattened polar projection with latitude lines drawn every 30° down to  $-30^\circ$ . Radial tick marks mark the observed phases. The darkest regions correspond to a temperature 870 K below the photospheric value.

Due to the long period and limited time span of each observing run, the data were phased from three consecutive rotations ( $\approx 30$  days) of the star.

### 3. Doppler imaging the stellar photosphere

#### 3.1. Spectral lines for imaging

Doppler images were derived using four spectral lines: Fe I 6430 Å, Ca I 6439 Å, Fe I 6643 Å and Fe I 6678. Synthetic local line profiles were generated using Kurucz's model atmospheres (Kurucz 1979) assuming an effective temperature of 5000 K. A macro-turbulent velocity of  $4 \text{ km s}^{-1}$  and a micro-turbulent velocity of  $2 \text{ km s}^{-1}$  were also used in the modeling. The image reconstruction was performed using the maximum entropy method, the details of which can be found in Vogt, Penrod, & Hatzes (1987).

**Table 1.** Spectroscopic observations for HD 106225

JD 244	Exp (min)	S/N	Phase
9767.962	40	145	0.075
9768.914	50	270	0.166
9769.972	50	220	0.268
9729.033	30	130	0.371
9729.962	60	150	0.417
9771.825	60	250	0.447
9730.993	45	130	0.516
9793.879	45	210	0.570
9795.892	80	300	0.764
9796.876	100	375	0.858

#### 3.2. Stellar parameters

The projected rotational velocity of HD 106225 was measured by fitting a synthetic spectral line profile to the mean (averaged over all observations) profile of the lines used for Doppler imaging. The mean value determined from the individual lines was  $25 \pm 1 \text{ km s}^{-1}$ , identical to the value derived by Fekel et al. (1991). Fig. 1 shows the mean profile of the four lines (crosses) and the synthetic fit (lines) from a rotating star without spots.

The stellar inclination of HD 106225 was derived by varying the input inclination until the misfit between observed and computed spectral line profiles ( $\chi^2$ ) was minimized. This occurred at an inclination of  $55^\circ$  which was used in all the Doppler reconstructions. S94 inferred an inclination in the range  $52^\circ < i < 78^\circ$  based on estimates of the stellar radius, companion mass, and the fact that the system is non-eclipsing.

#### 3.3. The images

Figs. 2-5 show the individual Doppler images derived from the Fe I 6430 Å, Ca I 6439 Å, Fe I 6643 Å, and Fe I 6678 Å lines, respectively. These are all shown in a flattened polar projection. Latitude lines occur at equally-spaced intervals down to a latitude of  $-30^\circ$ . The dark circle represents the stellar equator. Radial tick marks indicate the observed phases. All images are

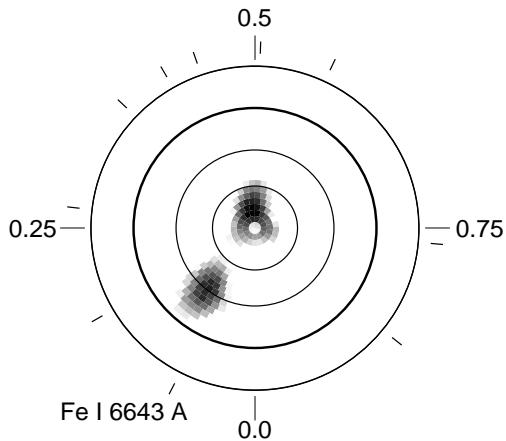


**Fig. 4.** The Doppler image derived using the Fe I 6643 Å line. Darkest regions are 650 K below the photospheric temperature.

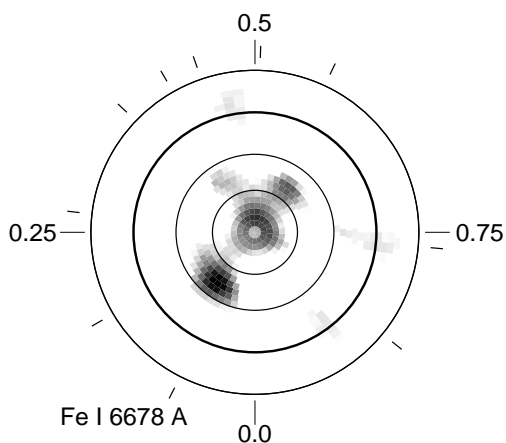


**Fig. 5.** Doppler image derived using Fe I 6678 Å. Darkest regions are 870 K below the photospheric temperature.

consistent in that they show a polar spot with an appendage at phase 0.5 and a high-latitude spot that is detached from the polar spot.

Representative observed spectral line profiles and fits are shown only for the Fe I 6430 Å and Ca I 6439 Å lines in Figs. 6 and 7. Observed profiles are shown as vertical marks whose length indicates the error in the flux profile. The predicted spectral line profiles from the individual Doppler images are shown as lines. Fig. 8 shows the Doppler image in stereographic projection produced by averaging the individual maps in Figs. 2–5.

The image of HD 106225 for 1995.14 has strong similarities to the image shown in S94 derived for the epoch 1991.3. (Note that the longitude convention of S94 has the star rotating in the opposite sense from the images presented here, i.e. orbital phase decreases with the stellar longitude of the S94 image.) That distribution showed a large, high latitude spot near phase 0.15 and latitude +50° that was attached to the polar spot along with another polar appendage at latitude +60 to +75° and phase 0.63.

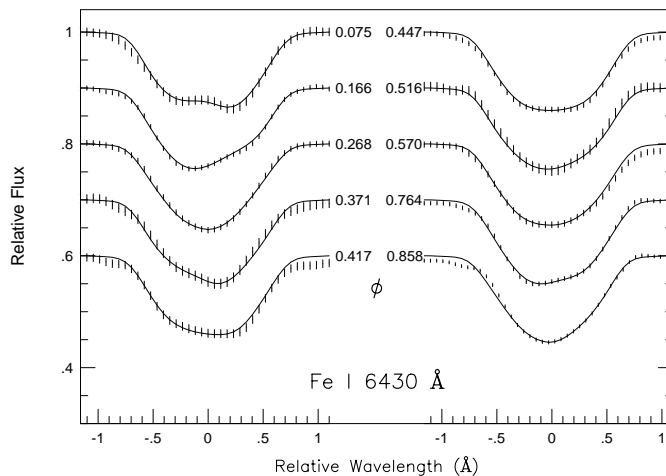


**Fig. 6.** The observed spectral line profiles (vertical bars) for Fe I 6430 Å and the predicted profiles (lines) from the Doppler image. The length of each vertical bar is an indication of the error in the flux measurement.

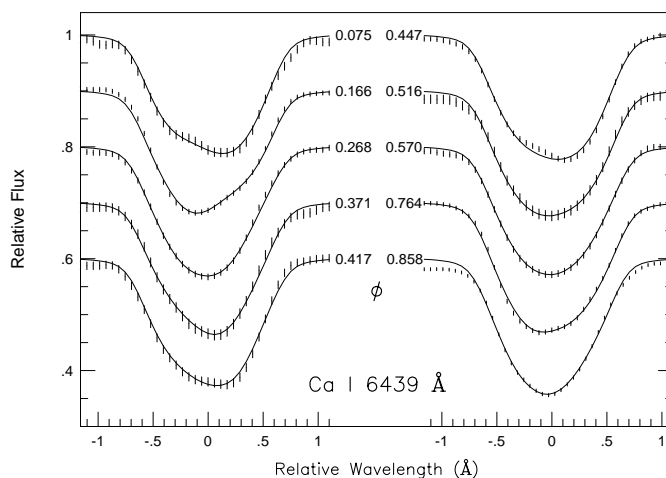


**Fig. 7.** The observed spectral line profiles (vertical bars) for Ca I 6439 Å and the predicted profiles (lines) from the Doppler image used in the reconstruction

#### 4. H $\alpha$ variations

S94 presented H $\alpha$  profiles spanning a complete rotation period and these showed a rather complicated behavior. Strassmeier was able to identify three distinctive features in the overall profile shape: a blue-shifted (by about 50 km s<sup>-1</sup>) emission component, a central sharp absorption feature, and a broad red-shifted absorption feature. Many of these same features can be seen in the H $\alpha$  profiles in 1995 which are shown as a function of phase in Fig. 9. The variations are quite complex going from almost pure H $\alpha$  absorption near phase 0 to complete emission half a rotation later. The horizontal dashed line marks the location of the central wavelength of H $\alpha$ . Note the presence of the central absorption component even when H $\alpha$  is strongly in emission. This self-reversal in the H $\alpha$  emission is often seen in

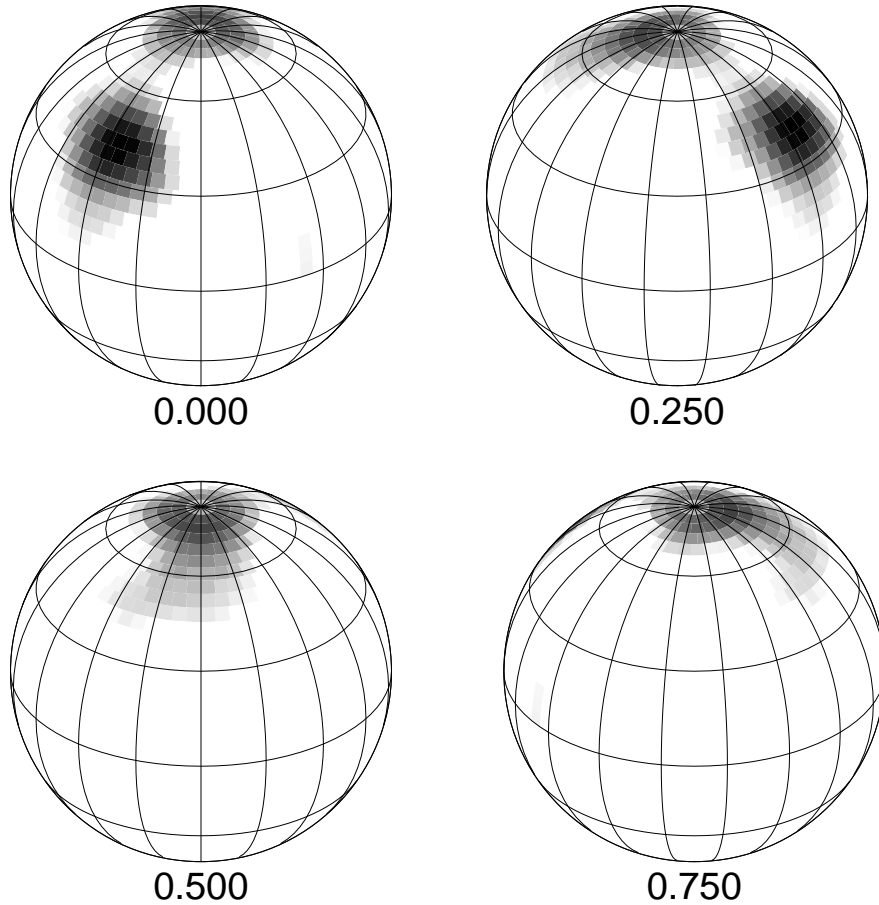


**Fig. 8.** The average Doppler image shown at 4 rotation phases in stereographic projection.

very active stars (e.g. Panagi et al. 1991; Hatzes 1995) and it is a normal characteristic of emission profiles formed in an optically thick chromosphere (e.g. Houdebine et al. 1995; Houdebine & Doyle 1994; Hawley & Fisher 1992).

There are, however, some subtle differences between the behavior of the  $H\alpha$  profiles in 1991 and 1995. These include: 1) The broad, red-shifted emission feature which is clearly visible at rotation phase 0.856 in S94 is almost gone in 1995. 2) The blue shifted emission feature was almost absent between phases 0.26 and 0.37 in 1991, but is still quite strong at these phases in 1995. 3) The sharp absorption feature seen near the time the center of mass of the system transits ( $\phi = 0.77$ ) was not seen. Strassmeier did mention that this observation may have been contaminated by moonlight, but even so, S94 shows absolutely no emission at this phase whereas in 1995 HD 106225 showed very strong  $H\alpha$  emission with a strong central absorption component. 4) Finally, phase 0.45 in 1995 showed a red-shifted emission peak which was not present in S94. In spite of these differences, the overall temporal behavior of  $H\alpha$  in 1995 is qualitatively similar to that which was observed by S94.

The full emission  $H\alpha$  profiles were generated by subtracting of a reference spectrum of  $\alpha$  Boo that was convolved to the same rotational velocity as HD 106225. The radial velocity of the flux centroid of the  $H\alpha$  residual emission profile was measured with respect to the photospheric absorption lines. These radial velocity measurements are shown in Fig. 10 phased to

the rotation period. There is clear evidence of sinusoidal variations with an amplitude  $10 \text{ km s}^{-1}$ , significantly less than the projected rotational velocity of the star. If the  $H\alpha$  emission responsible for this modulation originates from a surface feature such as plage, then this radial velocity variability is consistent with this feature located at high ( $\approx 70^\circ$ ) latitude.

### 5. Differential rotation in HD 106225

S94 estimated the differential rotation of HD 106225 by comparing the Doppler image to the spot distribution derived from photometry spanning the 1991 observing season and found that the differential rotation for HD 106225 was at least 10 times less extreme than on the Sun and in the opposite sense; the poles of HD 106225 rotated faster than the equator. Such polar acceleration has been seen on the RS CVn star HR 1099 (Vogt et al. 1997) and UX Arietis (Vogt & Hatzes 1991). The preliminary differential law derived by S94 was

$$\Omega = 34.17 + 0.78 \sin^2 \ell \quad (2)$$

where  $\ell$  is the stellar latitude.

The differential rate can be defined by the parameter

$$\alpha = \frac{\Omega_{equator} - \Omega_{pole}}{\Omega_{equator}} \quad (3)$$

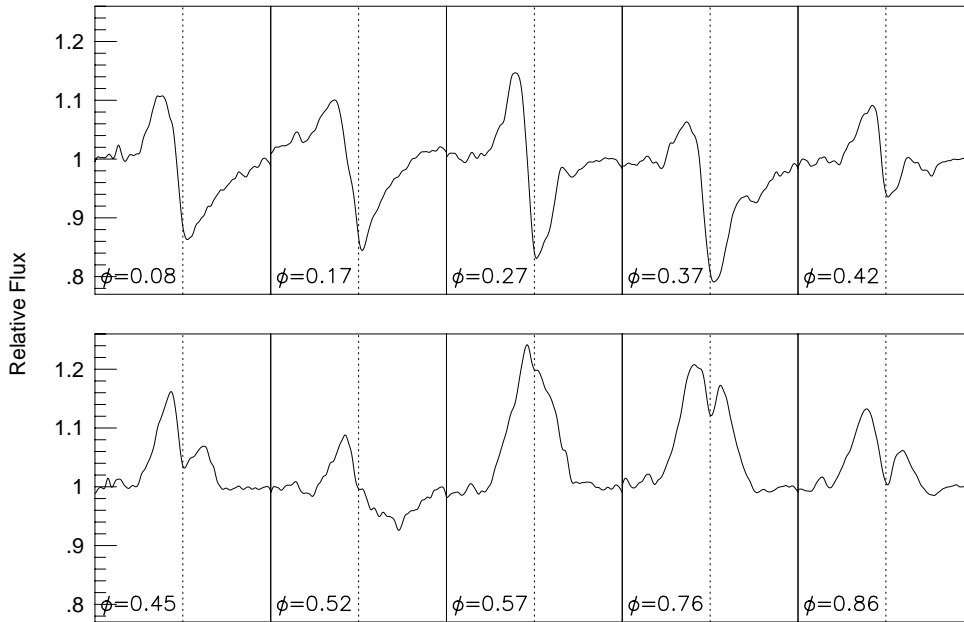


**Fig. 9.** Observed  $H\alpha$  line profiles as a function of orbital phase. The dashed line represents the center of  $H\alpha$  as measured with respect to the photospheric lines.

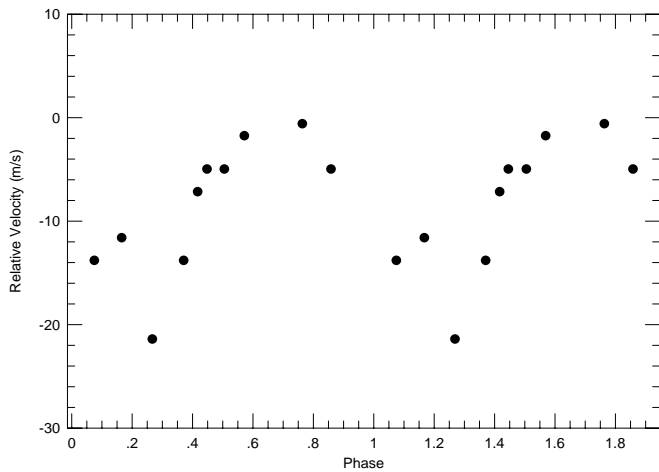


**Fig. 10.** The radial velocity variation of the  $H\alpha$  emission profile after subtracting underlying absorption profile. Points are repeated for the second cycle.

The S94 rotation law (Eq. 2) yields a value of  $\alpha = -0.0228$ . (S94 defined  $\alpha$  using the rotation rates at the equator and latitude =  $45^\circ$ . In this paper the “pole” is defined as latitude =  $90^\circ$  and the S94 value of  $\alpha$  was recalculated accordingly.)

One cannot, of course, derive the differential rotation on HD 106225 based on two images (S94 and this work). Not only is there considerable uncertainty in the identification of common features between the two images, but there is also the ambiguity as to whether a spot feature rotates faster or slower than the orbital period. However, by combining the two images with the photometric modelling of S94 one can at least see if the spot configuration on HD 106225 in 1995 is consistent with the differential rotation law derived by S94.

Table 2 lists the location of spot features found by S94. Spot A, B, and C are labeled in the same convention as S94. Spot C was one whose presence was inferred from modeling of the photometric light curve, consequently its latitude is not known. Spot ‘D’ was a polar appendage in the Doppler image that was not discussed by S94. Table 3 lists the major spot features for 1995.0

S94 inferred a migration rate of  $-0.16^\circ/\text{day}$  and  $+0.1^\circ/\text{day}$  for spots 91A and 91B, respectively (91A rotates slower than the orbital period and 91B rotates faster). Using these migration rates results in a predicted location of  $\phi = 0.33$  (for 91A) and  $\phi = 0.71$  (for 91B) in 1995.0. Spot 91D has the same latitude as 91B so it is reasonable to expect that it has the same migration rate as 91B. This results in a predicted location of  $\phi = 0.41$  in 1995.0. The latitude of 91C was unknown since it was inferred from photometry and was believed to have emerged after the time of the S94 Doppler imagery. Doppler imaging studies of the RS CVn star HR 1099 indicate that spots emerge near the equator (Vogt et al. 1997) so it is assumed that this is the case for the new spot features on HD 106225. If indeed this feature lies at low latitude than the migration rate for 91A would be more appropriate and this yields a predicted location of  $\phi = 0.08$  for 91C in 1995.0

The spot features in the 1995.0 image that are nearest to the predicted locations are 95B (for 91A), 95C (for 91B) and 95A (for 91C). (Spot 95C is a very short polar appendage seen in the average Doppler image of Fig. 8.) Table 1 lists time derivative of the phase location and the mean latitude of the features used for deriving the differential rotation. A least squares fit to the data yields a rotation law of

$$\Omega = 34.139 + 0.70 \sin^2 \ell \quad (4)$$

**Table 2.** Spot locations in 1991.3

Spot	Phase	Latitude
91A	0.88	40°
91B	0.38	60°
91C	0.61	?
92D	0.06	75°

**Table 3.** Spot locations in 1995

Spot	Phase	Latitude
95A	0.10	40°
95B	0.52	60°
95C	0.78	75°

**Table 4.** Rotation rates of spot features

1991	1995	$d\phi/dt$ (deg/day)	$\Omega$ (deg/day)	$\ell$	$\sin^2\ell$
91A	95B	+0.10	34.556	53	0.63
91B	95C	-0.17	34.826	80	0.77
91C	95A	+0.15	34.507	45	0.50

with a correlation coefficient of  $R = -0.94$ . (Of course with a line fit through only 3 points one is more likely to get a high degree of correlation.) This results in a value of  $\alpha = -0.0205$ .

A word of caution is in order regarding this differential rotation law. Although it is consistent with the one derived by S94, it is based on the proper identification of spot features from two Doppler images separated by nearly four years in time. The corresponding spot features between the two maps may have been misidentified, or the spots seen in the 1995 image may be completely different from the ones shown in S94. The true differential rotation law on HD 106225 may be entirely different to the one derived here. Clearly, a sequence of Doppler images with better time resolution is needed to confirm this result.

## 6. Discussion

### 6.1. Chromospheric emission

The amplitude of the  $H\alpha$  radial velocity (RV) variations (Fig. 10) suggests a feature located at high ( $\ell \approx 70^\circ$ ) latitude. The overall shape of the RV curve is also consistent with a feature located at high latitudes. A low latitude feature would be on the back side of the star (and out of view) for about half a stellar rotation, yet the RV curve varies reasonably smoothly over a rotation period and is almost sinusoidal in shape. The  $H\alpha$  emission has maximum blue shift at phase 0.3 and maximum redshift (receding over the limb) at  $\phi = 0.7$ . If the mean value of  $10 \text{ km s}^{-1}$  is subtracted from the curve, then the  $H\alpha$  emission feature has “zero” radial velocity (i.e. crossing the line-of-sight) at  $\phi = 0.4$ . It is estimated that the location of the  $H\alpha$  emitting region responsible for the rotational modulation of the  $H\alpha$  profile is latitude  $70^\circ$  and phase 0.4. This would place this region adjacent to the polar extension seen in the Doppler image. This suggests that if plage is responsible for the rotational modula-

tion of the  $H\alpha$  emission, then it must be nearly, but not exactly co-spatial with the polar extension.

### 6.2. Spot morphology and migration

The Doppler images for most RS CVn stars show a spot morphology dominated by a large polar spot or cap. Although HD 106225 shows evidence for a polar cap, it appears to be considerably smaller ( $r \approx 15^\circ$ ) than those found on other RS CVn stars ( $r \approx 30^\circ$ ). A small polar cap is also evident in the mean spectral line profiles produced by averaging over a rotation period (Fig. 1). Although there is a slight flattening of the line core which is most likely due to a polar spot, for the most part the spectral lines have a mean shape very nearly that of a rotationally broadened profile from an unspotted star. It may be that we are viewing HD 106225 nearly equator-on and, as shown by Hatzes et al. (1996), RS CVn stars with high stellar inclinations tend to have less flattening of the stellar line cores. Although the inclination derived by Doppler imaging is  $55^\circ$ , this is uncertain by  $\pm 20^\circ$  so the true inclination may be higher. If true, then HD 106225 may have a much larger polar spot area, but it does not produce significant flattening of the line cores due to the low projected area. However, simulations indicate that the degree of line flattening in HD 106225 is not consistent with a large polar spot viewed at higher stellar inclinations, although one should be cautious about making geometrical comparisons between stars of different surface gravity, temperature, etc.

The small size of the polar spot on HD 106225 may related to the long period of the star. Sigma Geminorum is one of the few RS CVn-type stars on which a polar spot has not been found (Hatzes 1993) and interestingly this star has a rather long rotation period of 19.4 days. Doppler imaging of other long-period RS CVn stars are needed to establish any trend of polar spot area with rotation period.

Schüssler & Solanki (1992) proposed that the polar spot seen on many rapidly rotating active stars is due to the Coriolis force dominating over the buoyancy force on rising magnetic flux tubes. This causes the flux tube to rise along paths parallel to the star’s rotation rather than along radial paths. Further work on this by Schüssler et al. (1996) showed that for slowly rotating stars flux emerges at lower latitudes and that the mean latitude of emergence shifts to higher latitudes for increasing stellar rotation rates. Evidence in support of this is found in the spot morphology for RS CVn stars.

Fig. 11 shows the spot distribution on four RS CVn stars with different rotation periods. These are EI Eridani (image from 1990) with a period of 1.94 days, HR 1099 (image from January, 1997; see Vogt et al. 1997), HD 106225 (this work) with a period of 10.4 days, and  $\sigma$  Geminorum (image from 1992; see Hatzes 1993) with a period of 19.4 days. There appears to be a trend of decreasing polar spot area with rotation period along with the appearance of an active latitude band for  $\sigma$  Geminorum. This trend is consistent with the Schüssler et al. (1996) scenario, although more Doppler images, particularly for stars with long rotation periods are needed to establish this trend. Furthermore, several images spanning several years are needed for each star

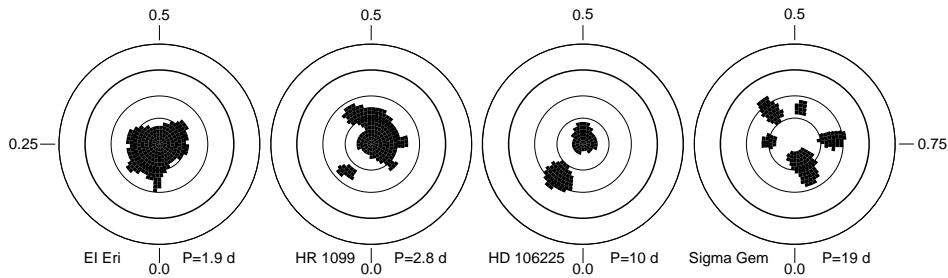


**Fig. 11.** Doppler images for 4 spotted stars with different rotation periods: EI Eridani (1.94 d), HR 1099 (2.83 d), HD 106225 (10.4 d), and  $\sigma$  Geminorum (19.4 d).

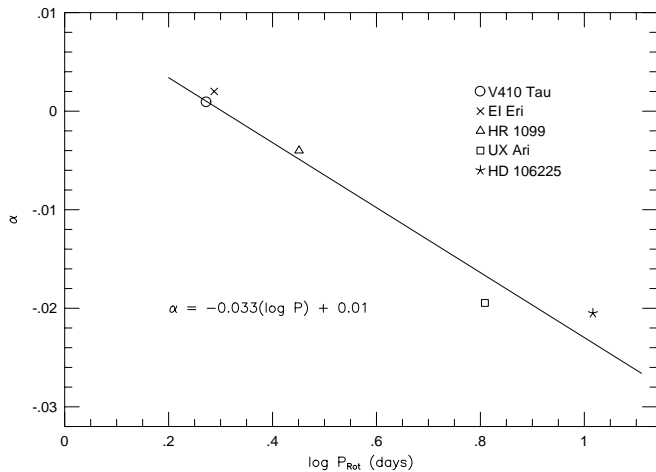


**Fig. 12.** The differential rotation parameter,  $\alpha$ , as a function of  $\log P_{rot}$  for 3 RS CVn stars and one WTTS.

to ensure that a small polar spot, or active latitude band is not merely due to being at a particular phase in the activity cycle.

In a long term Doppler imaging study it was established that spots on HR 1099 emerge near the equator and that mid-latitude spots often migrate to higher latitudes and join with the polar spot (Vogt et al. 1997; Vogt & Hatzes 1996). We can see evidence for this occurring on HD 106225. The dominant spot in 1991 (91A) has decreased in size and shifted to higher latitudes by about  $20^\circ$  to appear as feature 95A in 1995. Because spot 91C in S94 was inferred from photometry the precise latitude of its emergence is unknown, but if the behavior is similar to HR 1099, then we may assume that this latitude is near the equator. If so, then this feature has also migrated towards the pole by about  $40^\circ$  in 3 years time. A Doppler image of HD 106225 in the epoch 1996-1997 may reveal this feature as a polar appendage.

### 6.3. Differential rotation in rapidly rotating stars

Differential rotation rates have now been estimated for 3 other RS CVn stars from Doppler tomography:  $\alpha = -0.004$  for HR 1099 (Vogt et al. 1997),  $\alpha = -0.02$  for UX Arietis (Vogt & Hatzes 1991), and  $\alpha = +0.002$  for EI Eridani (Hatzes & Vogt 1992). Rice & Strassmeier (1996) also estimated the differential rotation for the weak T Tauri star V410 Tau ( $\alpha = +0.001$ ). Fig. 12 shows these differential rotation rates as well as the one determined for HD 106225 plotted as a function of the logarithm

of the rotation period in days. The line represents a least squares fit of the form:

$$\alpha = -0.033 \log P_{Rot} + 0.01 \quad (5)$$

In spite of the sparse number of points, there appears to be a correlation in the differential rotation rates of spotted stars with rotation period: short-period spotted stars have differential rotation rates in the same sense as the Sun, but as the period increases the differential rotation rates becomes larger and in the opposite sense as the Sun, (i.e. the poles of the star rotate faster than the equator). The cross-over point between stars with polar acceleration and those with equatorial acceleration (i.e. solid-body rotation) is about 2 days. The differential rotation versus  $\log P$  relationship is consistent with that found through photometric studies. Hall (1991) has shown that shorter period stars exhibiting more solid body rotation.

Interestingly, the WTTS, which is single and young, also seems to lie on this trend. Tentatively this argues that rotation is the key ingredient for determining the differential rotation for stars of similar spectral type and that tidal forces do not play an important role in determining the differential rotation law. Clearly, differential rotation rates derived from Doppler imaging studies are needed for a much larger sample of stars before a real trend with rotation period can be established.

There are departures from the linear  $\alpha - P$  shown in Fig. 12. Foremost is the Sun, with a rotation period of 27 days ( $\log P = 1.43$ ) and  $\alpha \approx 0.2$ , it clearly would not lie on the linear relationship of Fig. 12. There are two other spotted stars which do not lie on the relationship defined by Eq. 5. The young star AB Dor, with a rotation period of 0.51 days ( $\log P = -0.29$ ) and  $\alpha = +0.0046$  (Donati & Collier Cameron 1997), does follow the trend of shorter period stars having more positive  $\alpha$ , but it departs significantly from the law defined by Eq. 5. At the present time it is not known if  $\alpha$  is merely a more complicated function of the rotation period or whether the discrepant  $\alpha$  values actually are indicative of a different dynamo mechanism at work. Clearly, differential rotation rates of more stars, particularly the long-period ones, are needed before we can fully understand the role the rotation period plays in the differential rotation rate of the star.

*Acknowledgements.* This work was possible under the support of NSF grant AST-9315115. I wish to thank the referee, Klaus Strassmeier, for his valued comments and for pointing out other differential rotation determinations.

## References

- Bidelman, W.P. 1981, AJ, 86, 553.
- Donati, J.-F. & Collier Cameron, A. 1997, MNRAS, in press.
- Fekel, F.C. 1991, AJ, 101, 1489.
- Hall, D.S. 1991, in IAU Colloq. 130, *The Sun and Cool Stars: Activity, Magnetism, and Dynamos*, ed. I. Tuominen, D. Moss, G. Rüdiger, (Springer-Verlag: Berlin) p. 354.
- Hatzes, A.P. 1993, ApJ, 410, 777.
- Hatzes, A.P. 1995, ApJ, 451, 784.
- Hatzes, A.P. & Vogt, S.S. 1992, MNRAS, 258, 387.
- Hatzes, A.P., Vogt, S.S., Ramseyer, T.F., & Misch, A. 1996, ApJ, 469, 808.
- Hawley, S.L. & Fisher, G.H. 1992, ApJS, 78, 565.
- Houdebine, E.R. & Doyle, J.G. 1994, A&A, 289, 185.
- Houdebine, E.R., Doyle, J.G., & Kościelicki 1995, A&A, 294, 773.
- Kurucz, R.L. 1979, ApJS, 40, 1.
- McCarthy, J., Sandiford, B., Boyd, D. & Booth, J. 1993, PASP, 105, 881.
- Panagi, P.M., Byrne, P.B., & Houdebine, E.R. 1991, A&AS, 90, 437.
- Rice, J.B. & Strassmeier, K.G. 1996, A&A, 316, 164.
- Schüssler, M. & Solanki, S.K. 1992, A&A, 264, L13.
- Schüssler, M., Caligari, P., Ferriz-Mas, A., Solanki, S.K., & Stix, M. 1996, A&A, 314, 503.
- Strassmeier, K.G. 1994, A&A, 281, 395.
- Vogt, S.S. & Hatzes, A.P. 1991, in IAU Colloq. 130, *The Sun and Cool Stars: Activity, Magnetism, and Dynamos*, ed. I. Tuominen, D. Moss, G. Rüdiger, (Springer-Verlag: Berlin) p. 297.
- Vogt S.S., Penrod G.D., & Hatzes A.P., 1987, ApJ 321, 496
- Vogt, S.S. & Hatzes, A.P. 1996, in Proceedings of IAU Symposium No. 176: Stellar Surface Structure, eds. K.G Strassmeier & J.L. Linsky (Kluwer Academic Publishers, Dordrecht) p.245.
- Vogt, S.S., Hatzes, A.P., Misch, A., & Kürster, M. 1997, ApJS, submitted.